E83-10353

NASA

Technical Memorandum 85046

SEASAT Observations of Lithospheric Flexure Seaward of Trenches

David C. McAdoo and Chreston F. Martin

JUNE 1983

National Aeronautics and
Space Administration

Goddard Space Flight Center
Greenbelt, Maryland 20771

(E83-10353) SEASAT OBSERVATIONS OF LITHOSPHERIC FLEXURE SEAWARD OF TRENCHES (NASA) 52 p HC A04/MF A01 CSCL 05B

N83-29751

Unclas
G3/43 00353

TM 85046

SEASAT OBSERVATIONS OF LITHOSPHERIC FLEXURE SEAWARD OF TRENCHES

David C. McAdoo
Chreston F. Martin

June 1983

GODDARD SPACE FLIGHT CENTER
Greenbelt, Maryland 20771

ABSTRACT

Lithospheric flexure seaward of deep ocean trenches is evident in SEASAT altimeter observations of the marine geoid. In fact, mechanical models of lithospheric flexure can be tested directly on the SEASAT altimeter data. We have used a simple elastic model for the oceanic lithosphere and, after least squares adjustments, have recovered estimates of model parameters including Outer Rise (OR) amplitude, OR wavelength and effective lithospheric thickness.

Effective lithospheric thickness have been recovered for five regions: the Mariana, the Kuril, the Philippine, the Aleutian and the Middle America OR. These results support the suggestion of Bodine et al. (1981) that effective thickness, T, increases with age of lithosphere in approximate accord with the relation $T \cong C \bullet age^{1/2}$ where $C \cong 4$ km$\cdot$my$^{-1/2}$. In fact, our altimetric results agree more closely with this relation than do published results based on bathymetric data. The close agreement with the thickness-age relation suggests that there is no longer any need to assume that significant horizontal compression (cf. Bodine et al., 1981) acts across the Kuril, Marianas and Izu-Bonin trenches. This thickness-age relation implies that flexural strength of the oceanic lithosphere is temperature controlled.

CONTENTS

INTRODUCTION

The Outer Rise seaward of deep ocean trenches is generally attributed to flexure of the oceanic lithosphere prior to subduction. Various models have been proposed to describe this flexure. They all include a mechanically strong lithosphere - loaded from the arcward side of the trench axis - overlying a fluid-like asthenosphere. Simplest among them is the uniform elastic plate model which has been applied to Outer Rises by Hanks (1971), Watts and Talwani (1974), Parsons and Molnar (1976), Caldwell et. al. (1976) and others. Other models employ a viscous (DeBremaecker, 1977), a viscoelastic (Melosh, 1978) or an elastic - perfectly plastic lithosphere (McAdoo et. al., 1978). More complex models (Goetze and Evans, 1979; Chapple and Forsyth, 1979; Bodine et. al., 1981) include a variable rheology with depth and presumably yield more realistic estimates of flexural stresses in the lithosphere. We should note that elastic models of lithospheric flexure have been applied to phenomena other than Outer Rises by Gunn (1943) and Walcott (1970). For a comprehensive review of lithospheric flexure see Turcotte (1979).

Quite naturally these lithospheric models have been tested almost exclusively on bathymetric profiles. However, the Outer Rise also has a clear gravitational expression. Watts and Talwani (1974) showed that free-air gravity anomalies, which they referred to as the Outer Gravity High, have a shape and breadth which is similar to that of the underlying Outer Rise/slope complex. They also indicated

that the Outer Gravity High can be attributed largely to flexure of the oceanic lithosphere. Outer Gravity Highs have amplitudes as large as 60 mgal and wavelengths of several hundred kilometers. The gravity highs of course possess geoidal counterparts which have similar wavelengths and amplitudes as great as 6 meters. We shall refer to these as Outer Geoid Highs. The altimeter on the SEASAT satellite (see Tapley et. al., 1982) has made precise, direct observations of the marine geoid between $+72^{o}$ and -72^{o} latitude. These altimeter data provide dense, uniform coverage of all Outer Rises and are well suited to the task of directly testing lithospheric flexure models. Direct, altimetric observations of the Outer Geoid High also have the advantage that they are less affected by seamounts, variations in sediment thickness, etc. than are corresponding gravimetric and bathymetric observations. Due to their high accuracy and nearly global coverage, SEASAT data significantly augment available information concerning the Outer Rises.

In this paper we will be testing the elastic plate model by using the SEASAT altimeter data. Bodine et al. (1981) have found that the model of a uniform, thin elastic lithosphere overlying a fluid-like asthenosphere is adequate for describing flexure of the oceanic lithosphere. They reached this conclusion after comparing elastic model results with those from more complex, experimentally-constrained lithospheric rheologies (i.e., layered cataclastic - elastic - plastic). However, the more complex rheological models do produce more realistic stress estimates, and they produce lower estimates, in particular,

of stresses associated with horizontal compressive loads transverse to the trench. Based on their comparison of the elastic model with the complex rheological model, Bodine et al. (1981) were also able to postulate a relation between effective elastic thickness of the lithosphere and its age (see also Caldwell and Turcotte, 1979). We will also be using our results from SEASAT altimeter data to test this thickness-age relation.

MODEL OF OUTER SLOPE AND RISE

As indicated in the Introduction, flexure of oceanic lithosphere seaward of deep ocean trenches can be adequately modelled as an end-loaded elastic plate overlying a fluid asthenosphere. Using the same elastic plate model as that which was first applied to the Outer Rise problem by Hanks (1971) one obtains the following familiar expression for deflection, w, of the plate

$$w = w_o \sin\left(\frac{x}{\alpha}\right) \exp\left(-\frac{x}{\alpha}\right) \qquad (1)$$

where x is the horizontal coordinate normal to the trench axis, w is an amplitude parameter equal to $2^{1/2} \exp\frac{\pi}{4}$ times w_b, the outer rise height, and α is a measure of the flexural wavelength which can be related to rise crest position x_b by $\alpha = 4x_b/\pi$ (see Fig. 1). α can also be related to plate thickness, T_e, by

$$T_e = \left[\frac{3(1-\nu^2)g(\rho_m-\rho_w)}{E}\right]^{1/3} \alpha^{4/3} \qquad (2)$$

where E is Young's modulus, ν is Poisson's ratio, g is the acceleration of gravity and ρ_m and ρ_w are mantle and seawater densities. The deflection solution, (1), assumes the lithosphere to be loaded vertically; i.e., horizontal loading is negligible (see Caldwell et. al., 1976). For

computations, we will assume: $\rho_m = 3.3 \times 10^3$ kg·m^{-3}, $\rho_w = 1.0 \times 10^3$ kg·m^{-3}, $E = 6.5 \times 10^{10}$ N·m^{-2}, $\nu = 0.25$ and $g = 9.8$ m·sec^{-2}.

Of course this deflection of the lithosphere gives rise to gravity anomalies and geoid undulations. Furthermore, surface observations of gravity (see Watts and Talwani, 1974) suggest that the Outer Rise and outer trench slope are not isostatically compensated. Rather, observed gravity is consistent with a model (see Figure 1) of uncompensated topography wherein the crust and lithosphere deflect as a unit. The relationship - more specifically the admittance - between bathymetry and geoid heights derived from SEASAT data is also consistent with this model of uncompensated lithospheric flexure (see Appendix).

In order to derive the geoid undulations for this elastic plate model, two approaches have been tried. The first involves numerical integration. Geoid undulations arise due to density anomalies created by deflection of the seafloor and the Moho. The integral expression for these undulations is

$$\Delta N(x) = \frac{-2G}{g} \int_{-x_o}^{\infty} \left[\int_{d-w(\xi)}^{d} (\rho_c - \rho_w) \ell n R dz + \int_{d+t-w(\xi)}^{d+t} (\rho_m - \rho_c) \ell n R dz \right] d\xi + L(x) \qquad (3)$$

where

$$R = \sqrt{(x-\xi)^2+z^2}$$

In the above expression, d is undeflected seafloor depth, t is crustal thickness, $w(\xi)$ is given by equation (1) and L(x) is the contribution from mass landward of the trench axis ($x < -x_o$; see discussion of mirror image assumption below). Numerical integration of (3) gives results that are quite consistent with second approach - the analytical approximation represented by equation (8) below. However, the numerical integration approach is not computationally efficient, so we have adopted a second approach. We use a thin mass layer approximation developed by Ockendon and Turcotte (1977). Deflections, w(x), of the lithosphere shall be assumed to manifest themselves gravitationally as two mass layers, the first layer resiti g at depth d and possessing a variable mass per unit area

$$\sigma_u(x) = (\rho_c-\rho_w)\, w(x) \,, \qquad (4a)$$

the second layer residing at Moho depth, d + t, and possessing a mass per unit area

$$\sigma_\ell(x) = (\rho_m-\rho_c)\, w(x) \qquad (4b)$$

Ockendon and Turcotte (1977) represented geoid undulations due to thin mass layers with a series expansion in powers of relative thickness. Retaining first and second order terms in the expansion (see Haxby and Turcotte, 1978), the following expression for geoid undulations, $\Delta N(x)$, results

$$\Delta N(x) = \frac{-2G}{g}\left\{\int_{-\infty}^{\infty} \rho^{(1)}(\xi)\, \ell n\, \frac{(x-\xi)}{L} d\xi \ \ldots \right. \tag{5}$$

$$\left. - \pi\left[\rho^{(2)}(x) - \rho^{(1)}(x)(d+t)\right]\right\}$$

In the above, $\rho^{(2)}(x)$ and $\rho^{(1)}(x)$ are the equivalent source and dipole moment of mass per unit area and are given by

$$\rho^{(1)}(x) = \int_0^{d+t} \Delta\rho(x,z)dz \tag{6a}$$

$$\rho^{(2)}(x) = \int_0^{d+t^+} \int_0^{z'} \Delta\rho(x,z)dzdz' \tag{6b}$$

where

$$\Delta\rho(x,z) = \sigma_u(x)\delta(z-d) + \sigma_\ell(x)\delta(z-d-t)$$

and δ is the delta function. Combining equations 1, 4, 5, and 6 yields

$$\Delta N(x) = \frac{-2G}{g}\left\{(\rho_m-\rho_w)w_o \int_{-x_o}^{\infty} \sin\left(\frac{\xi}{\alpha}\right)\exp\left(\frac{-\xi}{\alpha}\right)\ln\left(\frac{x-\xi}{L}\right)d\xi\right.$$

$$+ (\rho_m-\rho_w)w_o \int_{-\infty}^{-x_o} \sin\left(\frac{-\xi-2x_o}{\alpha}\right)\exp\left(\frac{\xi+2x_o}{\alpha}\right)\ln\left(\frac{x-\xi}{L}\right)d\xi$$

$$\left. + \pi\, w_o \sin\frac{x}{\alpha}\exp\left(\frac{-x}{\alpha}\right)\left[(\rho_c-\rho_w)\,t + (\rho_m-\rho_w)d\right]\right\} \qquad (7)$$

In (7) the plate deflections, $w(x)$, are assumed to be symmetric about the trench axis $x = -x_o$ where $w(x)$ is given by (1). This mirror image assumption is a far better approximation of reality than is the simpler approximation $w(x) = 0$ for $x < -x_o$. If for simplicity one were to assume $w(x) = 0$ for $x < -x_o$ the second term in (7) would be dropped.

The two integrals in (7) can be evaluated exactly. The following expression for geoid undulations results:

$$\Delta N(x) = \frac{(\rho_m-\rho_w)Gw_o\alpha}{g}\cdot 2\exp\frac{x_o}{\alpha}\left[\cos\frac{x_o}{\alpha} - \sin\frac{x_o}{\alpha}\ln\frac{(x+x_o)}{L}\right] \ldots$$

$$- \exp\left(\frac{-x}{a}\right)\left(\cos\frac{x}{a} - \sin\frac{x}{a}\right)\left(\pi + \mathrm{Im}\left(E_1\left(\frac{(x+x_o)(-1+i)}{a}\right)\right)\right)\ldots$$

$$- \exp\left(\frac{-x}{a}\right)\left(\cos\frac{x}{a} + \sin\frac{x}{a}\right) \cdot \mathrm{Re}\left(E_1\left(\frac{(x+x_o)(-1+i)}{a}\right)\right)\ldots$$

$$+ \exp\frac{(2x_o+x)}{a}\left(\cos\frac{(2x_o+x)}{a} + \sin\frac{(2x_o+x)}{a}\right).\mathrm{Im}\left(E_1\left(\frac{(x+x_o)(1+i)}{a}\right)\right)\ldots$$

$$-\exp\frac{(2x_o+x)}{a}\left(\cos\frac{(2x_o+x)}{a} - \sin\frac{(2x_o+x)}{a}\right) \cdot \mathrm{Re}\left(E_1\left(\frac{(x+x_o)(1+i)}{a}\right)\right)\Bigg\}$$

$$- \frac{2\pi G}{g} w_o \sin\frac{x}{a} \exp\left(\frac{-x}{a}\right) [(\rho_m - \rho_w)d + (\rho_c - \rho_w)\, t] \qquad (8)$$

where $E_1(\xi)$ is the exponential integral given by

$$E_1(\xi) = \int_{\xi}^{\infty} \frac{e^{-u}}{u}\, dt$$

and ξ is, in general, a complex variable (see Abramowitz and Stegun, 1972, p. 228). Re( ) and Im( ) in (8) denote respectively the real and imaginary parts of the particular argument. This expression, (8), for geoid undulations due

to plate flexure can be compared directly with SEASAT altimeter height profiles from which a long wavelength geoid has been subtracted. This comparison can provide estimates of model parameters such as flexural wavelength, α (or equivalently plate thickness, T_e, see eqn. 2) or amplitude, w_o. Such estimates have been obtained in the Results section using the method of least squares. Construction of the normal equations for least squares requires expressions for partial derivatives of $N(x, w_o, x_o, \alpha, t)$ with respect to parameters α, w_o, x_o, and t. Analytical expressions for these partials are obtained by differentiating (8) with respect to the parameters which are being estimated.

SEASAT OBSERVATIONS

Segments of 102 SEASAT altimeter passes over six trench/Outer Rise complexes have been analyzed (see Figure 2a,b,c). For each trench the number of passes analyzed is as follows: Middle America, 14; Philippine, 12; Aleutian, 23; Mariana, 12; Izu-Bonin, 10; Kuril, 30. The sea surface height profiles obtained from these passes will be treated as geoid height profiles. If the oceans were completely passive, the mean sea surface that SEASAT observed would, by definition, coincide with the geoid. For this analysis, the ocean dynamic component of sea surface height is, in most instances, the major error source. Mesoscale oceanographic phenomena such as ring currents, eddies, etc., constitute the bulk of this oceanographic "noise". Long wavelength (>1000km) phenomena will have no effect as such wavelengths are not included in this analysis. Amplitudes of these mesoscale oceanographic features may exceed a meter in places (e.g., the Oyashio-Kuroshio confluence zone near the Kuril trench; see Cheney, 1977). In most places these amplitudes are substantially less than a meter. The precision of the actual sea surface height measurement - after GDR corrections - is about 10 cm (Tapley et al., 1982).

For comparison with the Outer Geoid High model (8), pass segments 100 sec (700 km) in length have been chosen. These pass segments cover exclusively oceanic lithosphere on the verge of subduction; the segments terminate at the trench axis. These 100 sec segments have been high-pass

filtered. This has been accomplished by removing a degree-and-order 48 background geoid. The background geoid chosen is a truncation of an updated version (Frey and Klosko, 1983) of GEM 10C (Lerch et al., 1981) which uses Rapp's (1982) SEASAT - derived gravity anomalies at high degrees and orders. This high pass filtering, of course, removes unmodelled long wavelength effects including geoid signals associated with the subducting slabs and the thickening of the thermal lithosphere with age.

RESULTS

The 102 SEASAT pass segments of sea surface heights which are described in the Observations section above (see Figure 2a,b,c) have been fitted with the flexural model given by Equation (8). The method of least squares was used to recover estimates of three model parameters plus a bias (or vertical offset) parameter for each pass. The three model parameters are the flexural wavelength, α, the amplitude, w_b, and the trench axis position, x_o. Efforts were made to recover a fourth model parameter - crustal thickness or Moho depth, t; these efforts were not successful. This can be attributed to the fact that the model results (8) are rather insensitive to crustal thickness.

One or two representative passes from each of the six trenches are shown in Figures 3a-3i; both the SEASAT profile and the best-fitting model result are shown. Table I summarizes average values of model parameters, α and w_b, derived from the SEASAT passes over each of the six regions. We will discuss the Aleutian region in detail, below; the other five regions will be discussed briefly.

1. Aleutian Trench

Twenty-three SEASAT passes across the central Aleutian trench (see Figure 2a) have been analyzed. The individual estimates of flexural wavelength, α, that were obtained

after least squares adjustments, are shown in Figure 4a. The values of α which are shown in Figure 4a have not been corrected for non-perpendicularity of the SEASAT groundtrack to the trench axis. This geometric correction is accomplished by multiplying α_u times the $\sin\phi$ where ϕ is the angle between the groundtrack and the trench axis. For Aleutian passes this geometric correction is essentially negligible (i.e., $\phi \sim 90^{\circ}$). Note in Figure 4a that α varies only slightly from pass to pass, which is consistent with the small "formal" errors.

The least squares adjustment procedure was also used to independently recover estimates of the same three model parameters, α, w_o, and x_o, plus a bias parameter for the interpolated bathymetry profiles which coincide with the 23 SEASAT passes. The recovered values of flexural wavelength, α, are plotted in Figure 4b. Although there is fair agreement, particularly west of the Amlia fracture zone, between the bathymetrically and altimetrically derived flexural wavelengths, the scatter in the 23 values obtained from bathymetry is significantly greater than that exhibited by the values derived from SEASAT. Caldwell et al. (1976) obtained a value of α = 67 km from a SEAMAP13 shiptrack bathymetry profile across the Aleutian trench. This shiptrack value is shown in Figure 4b for comparison with interpolated profiles. It is clearly consistent with interpolated profiles in the vicinity. A nearby SEASAT profile, rev 582 (see Figure 3a), yields an estimate of α = 91.8 km which is significantly larger than Caldwell et al.'s (1976) estimate from bathymetry. In general estimates derived from bathymetry are significantly less

consistent from pass to pass than are those derived from SEASAT. Furthermore, the estimates of α which we obtained from bathymetric fits have a tendency - to be less than those derived from altimetry. This tendency is exhibited at other trenches and is discussed below. Seamounts, sediments and other localized topographic variations act as noise obscuring the Outer Rise; these same noise sources are significantly attenuated in the geoid signal, i.e., the Outer Geoid High. In some places, as discussed below, an Outer Geoid High is evident in the SEASAT data where an Outer Rise can not be found in the bathymetry.

As an indication of the good agreement between the model and the SEASAT data, it should be noted that the rms difference between model and data ranges from 22 to 40 cm for the 23 Aleutian passes. For rev 1185 (see Figure 3b) - the westernmost of the 23 - the rms difference is 22 cm which is not much larger than the measurement precision of SEASAT.

The Amlia fracture zone intersects, obliquely, the Aleutian trench between 186° and 187° E. This fracture zone - and possibly its down-slab extension - could be acting as a line of weakness in the lithosphere. It appears, in any case, to be affecting the Outer Rise and the Outer Geoid High. Therefore, the three SEASAT passes, revs 654, 166 and 1156 (dashed in Figure 2a), which intersect the trench between 186° and 187° E are excluded from the ensemble of 20 passes used to construct mean values of model parameters, α and w_o, in Table I.

2. Kuril Trench

Thirty ascending passes of SEASAT data across the Kuril trench were analyzed. However, the eight southwesternmost passes of these 30 were culled before regional mean values of α and w_o were computed for Table I. These eight passes cover (see dashed groundtracks in Figure 2a) Outer Rise which is influenced by subduction at the Japan trench as well as the Kuril trench. The Japan trench axis is oriented at roughly a 45° angle to the groundtracks of these passes - whereas the Kuril trench is nearly perpendicular to them. The high values (range 118 to 136 km) of flexural wavelength, α_u, (uncorrected for groundtrack geometry) are probably due to the influence of the Japan trench. It is also conceivable that high mesoscale variability in this region (see Observations section above, Cheney, 1977) might also be affecting these passes.

Recovered values of flexural wavelength, α, for the remaining 22 SEASAT passes across the Kuril trench range from 88 to 106 km with a mean of $\bar{\alpha}$ = 96 km. Using 10 shiptracks of bathymetric data, McAdoo et al. (1978) recovered values which range from 67 to 102 km with a mean of 89 km. As in the case of the Aleutians, the altimetrically derived estimates of α are more consistent from pass to pass than are the bathymetrically derived estimates. Furthermore, the maximum values recovered for both the Kuril and the Aleutian regions from SEASAT data nearly equal those from bathymetry. Once again, it appears

then that bathymetry tends to produce low estimates of flexural wavelength α. We will discuss this further, below. Figure 3c shows a representative pass, rev 469, across the Kuril trench. For this pass α is estimated to be 102 km and the rms difference between model and SEASAT profile is 52 cm; this rms difference ranges between 20 and 55 cm for the 22 passes.

3. Middle America Trench

Passes on or northwest of the Tehuantepec ridge were also analyzed but discarded inasmuch as these passes traversed the crest of the East Pacific Rise and produced results that were not consistent from one pass to the next. On the other hand, all descending SEASAT passes between the Tehuantepec and Cocos ridges (see Figure 2b), excluding redundant coincident passes, were analyzed and retained. These passes were fourteen in number.

These fourteen passes produce quite consistent results. The mean flexural wavelength, $\bar{\alpha}$, (before slight correction for groundtrack geometry) is 73.8 km for this sample of fourteen; the standard deviation is 4.4 km. Rev 558 is shown in Figure 3d as a representative of sea surrace and model geoid heights. The rms difference between model and observation for 558 is 28 cm; the rms differences for the rest of the passes range between 16 and 47 km. It should also be noted that we were not able to estimate flexural wavelengths for the interpolated bathymetric profiles along many of these 14 groundtracks as they did not even display an Outer Rise.

4. Philippine Trench

Eight SEASAT passes which traverse the Outer Rise seaward of the Philippine trench were analyzed. The resulting estimates of flexural wavelength were less consistent from pass to pass than similar estimates for other trenches. The mean value of flexural wavelength (uncorrected for groundtrack geometry) is 120.0 km and the standard deviation is 14.5 km. These passes are oriented at approximately a 34^{o} angle with respect to the trench axis (see Figure 2c); therefore, the geometric correction is large. Two SEASAT profiles, rev 578 and 736, are shown in Figures 3e and 3f. The agreement between model and observation is particularly good for rev 578; the rms difference is 13 cm. It is interesting to note that coincident profiles of interpolated bathymetry yield poor results; some passes exhibited no Outer Rise and the recovered flexural wavelength estimates, α_u (uncorrected for geometry), range from 50 to 127 km.

5. Izu-Bonin Trench

The presence of the Ogasawara Plateau and Ramapo Bank apparently interfere with development of a typical Outer Rise and Outer Geoid High adjacent to the southern Izu-Bonin trench. Bodine and Watts (1979) found that it is difficult to resolve an Outer Rise in shiptrack bathymetric profiles across this area. Only four SEASAT passes could reasonably

be analyzed and these were closely spaced. One of these, rev 664, is shown in Figure 3g. Note that in part because of the acute angle (32°; see Figure 2c) between groundtrack and trench axis, the Outer Geoid High is quite long. For the four passes, the mean value of uncorrected flexural wavelength, $\bar{\alpha}_u$, is 237.7 km. This uncharacteristically large value of $\bar{\alpha}_u$ (due to geometry plus an apparently thick lithosphere) necessitated using longer (128 sec) pass segments for this region. The corrected mean flexural wavelength is $\bar{\alpha}$ = 125.9 km.

Bodine and Watts (1979) found that it is difficult to estimate flexural wavelengths from shiptrack profiles of bathymetry across the Izu-Bonin trench. They handled this difficulty by assuming, a priori, a flexural wavelength, α (or x_b), which is consistent with a relation between age and effective lithospheric thickness. This a priori flexural wavelength is 90 km -- considerably less than our estimate from altimetry (126 km).

6. Northern Mariana Trench

Nine descending passes of SEASAT data across the northern Mariana trench were analyzed (see Figure 2c). Consistency of flexural wavelength estimates from pass to pass is poor. Because of the curvature of the trench, geometric corrections had to be applied individually to each pass. Due to a very acute angle between groundtrack and trench axis, three passes, revs 721, 477 and 233 (see dashed groundtracks in Figure 2c), were culled from an original

group of 12. A mean flexural wavelength (corrected for geometry) of 97.9 km (σ = 22.9 km) was estimated using nine passes. Interestingly, Bodine and Watts (1979) found that an Outer Rise was quite difficult to detect in shiptrack profiles of bathymetry across the northern Mariana. Two passes, revs 879 and 836, are shown in Figures 3h and 3i respectively. Rev 879 agrees quite well with the model (α_u = 128 km; rms of fit, 35 cm); rev 836 deviates substantially from the model (α_u = 107 km; rms of fit, 94 cm) due to the effect of two large seamounts in the western Marcus ridge.

INTERPRETATION

Bodine et al. (1981) applied a more realistic, complex rheological model of oceanic lithosphere to the phenomena of the Outer Rise. They resorted to a three-layer rheology - the shallowest layer being cataclastic, the next elastic and the deepest plastic. Rock mechanics experiments by Goetze and Evans (1979) on olivine were used to constrain characteristics of the plastic layer. Bodine et al. (1981) found that the Outer Rise shape predicted by this complex rheological model was not significantly different than that predicted by the simple elastic plate model with similar plate thickness. In fact, they were able to use the complex model to predict how the effective elastic thickness of oceanic lithosphere should depend on temperature and hence age. Using the model of Parsons and Sclater (1977) to describe the thermal evolution of the lithosphere, Bodine et al. (1981) postulated that the effective elastic thickness of the lithosphere, T_e, is given by

$$T_e = C \cdot age^{1/2} \qquad (9)$$

where $C = 4.6 \pm 0.6$ km·my$^{-1/2}$. This thickness law, (9), was derived by using the results of Goetze and Evans (1979) from experiments on dry olivine. A wet dunite rheology led to a slightly lower value of C. The thickness law based on a dry olivine rheology is plotted in Figure 5.

For a simpler interpretation of the thickness-age law, one can think of the effective elastic thickness as simply the depth to a particular isotherm. Caldwell and Turcotte (1979) find the 700°C isotherm most suitable.

Our estimates of effective elastic thickness derived from SEASAT altimeter data are also plotted in Figure 5. These six estimates correspond to the six regions which we studied -- the Kuril, Aleutian, Middle America, Philippine, Mariana and Izu-Bonin. The estimates are also listed in Table I. They are derived from the estimates of mean regional flexural wavelength, $\bar{\alpha}$, by using equation (2).

The agreement between our results for these six areas and the thickness age relation, (9), is quite good. The agreement is in contrast to the rather rough fit obtained using estimates derived from bathymetric data. This rough fit as depicted in Figure 10 of Bodine et al. (1981) is mostly a result of the low estimates of α and T_e obtained from bathymetric profiles across the Kuril, Izu-Bonin and Mariana trenches. Recall that we indicated in the Results Section that bathymetry, in contrast to altimetry has an apparent tendency to yield low estimates of T_e or α. Bodine et al. (1981) explained these low estimates of T_e from bathymetry by postulating that horizontal compression is acting across these trenches (Kuril, Izu-Bonin and Mariana); they suggested that this compression (1 kbar) reduces the effective thickness. They use the complex rheological model - as opposed to the simple elastic model - to describe this reduction in effective thickness. The complex rheological model is also very useful for producing

realistic estimates of stress and explaining certain steep outer trench slopes. If our thickness estimates, T_e, from altimetry as depicted in Figure 5 are valid, then it is not necessary to invoke horizontal compressive loads of this magnitude (1 kbar) across the three trenches.

DISCUSSION

SEASAT altimeter data over Outer Rises apparently provide better estimates of effective lithospheric thickness than do bathymetric data. We base this observation on the fact that altimetric results in a given region are more consistent from profile to profile. We have also suggested that bathymetric profiles across Outer Rises have a tendency to occasionally produce values of flexural wavelength - or plate thickness which are significantly less than corresponding estimates from SEASAT data.

We can speculate about reasons for this apparent superiority of altimeter data as an estimator. Altimeter data enjoys the advantage of the geoidal representation in which unmodeled, high frequency effects such as seamounts are attenuated. At present, however, we do not fully understand this discrepancy between altimetric and bathymetric estimates of plate thickness.

Regarding bathymetric profiles across Outer Rises, Jones et al. (1978) showed that the confidence limits on estimates of flexural (or plate thickness) are, in some cases, quite broad -- leading to uncertain estimates. Agnew and Sharman (personal communication, 1983) found that this uncertainty is sufficient in certain cases to permit only estimation of a lower bound on plate thickness.

CONCLUSIONS

SEASAT altimeter data provide significant new information on the deformation of the lithosphere seaward of deep ocean trenches. These data, when compared with a mechanical model, produces estimates of the effective elastic thickness of the lithosphere which are more consistent from profile to profile in a given region than those derived from bathymetry. For the six trenches which we studied, the effective elastic thickness derived from altimetry increases with the square root of lithospheric age as predicted by Bodine et al. (1981). Significant horizontal compression across these trenches is not indicated. This is consistent with Forsyth's (1982) studies of Outer Rise earthquakes from which he concluded that regional compressive stresses must be a small fraction of the bending stresses.

REFERENCES

Abramowitz, M. and I.A. Stegun, Handbook of Mathematical Functions, Dover, New York, 1972.

Bodine, J.H. and A.B. Watts, Lithospheric flexure seaward of the Bonin and Mariana trenches, Earth and Planet. Sci. Lett., 43, 132-148, 1979.

Bodine, J.H., M.S. Steckler and A.B. Watts, Observations of flexure and of the oceanic lithosphere, J. Geophys. Res., 86, 3695-3707, 1981.

Caldwell, J.G., W.F. Haxby, D.E. Karig and D.L. Turcotte, On the applicability of a universal elastic trench profile, Earth Planet. Sci. Lett., 31, 239, 1976.

Caldwell, J.G. and D.L. Turcotte, Dependence of the thickness of the elastic oceanic lithospheric on age, J. Geophys. Res., 84, 7572-7576, 1979.

Chapple, W.M. and D.W. Forsyth, Earthquakes and the bending of plates at trenches, J. Geophys. Res., 84, 6729-6749, 1979.

Cheney, R.E., Synoptic observations of oceanic frontal system east of Japan, J. Geophys. Res., 82, 5459-5468, 1977.

De Bremaecker, J.C., Is the oceanic lithosphere elastic or viscous, J. Geophys. Res., 82, 2001-2004, 1977.

Forsyth, D.W., Determinations of focal depths of earthquakes associated with the bending of oceanic plates at trenches, Phys. Earth Planet. Int., 28, 141-160, 1982.

Frey, H. and S. Klosko, An improved crustal gravity model for comparison with Magsat data, (abstract), 5th Ann. NASA Geodynamics Program Conference, p. 25, 1983.

Goetze, C., and B. Evans, Stress and temperature in the bending lithosphere as constrained by experimental rock mechanics, Geophys. J. R. Astron. Soc., 59, 463-478, 1979.

Hanks, T.C., The Kuril Trench - Hokkaido Rise system: Large shallow earthquakes and simple models of deformation, Geophys. J. R. abstr. Soc. 23, 173-189, 1971.

Haxby, W.F. and D.L. Turcotte, On isostatic geoid anomalies, J. Geophys. Res., 83, 5473-5478, 1978.

Jones, G.M., T.W.C. Hilde, G.F. Sharman and D.C. Agnew, Fault patterns in outer trench walls and their tectonic significance, J. Phys. Earth, 26, Suppl., S 85-5 101, 1978.

Lerch, F.J., S.M. Klosko, and B.H. Putney, Goddard earth models for oceanographic application (GEM 10B and 10C), Mar. Geod., 5(2), 2-43, 1981.

McAdoo, D.C., J.G. Caldwell and D.L. Turcotte, On the elastic - perfectly plastic bending of the lithosphere under generalized loading with application to the Kuril Trench, Geophys. J.R. astr. Soc., 54, 11-26, 1978.

McKenzie, D.P. and C. Bowin, The relationship between bathymetry and gravity in the Atlantic ocean, J. Geophys. Res., 81, 1903-1915, 1976.

Melosh, H.J., Dynamic support of the outer rise, Geophys. Res. Lett., 5, 321-324, 1978.

Ockendon, J. and D.L. Turcotte, On the gravitational potential and field anomalies due to thin mass layers, Geophys. J.R. astr. Soc., 48, 479-492, 1977.

Oppenheim, A.V. and R.W. Schafer, Digital Signal Processing, Prentice-Hall, New Jersey, p. 553-555, 1975.

Parsons, B. and P. Molnar, The origin of outer topographic rises associated with trenches, Geophys. J.R. astr. Soc., 45, 707-712, 1976.

Parsons, B. and J.G. Sclater, An analysis of the variation of ocean floor bathymetry with age, J. Geophys. Res., 82, 803-827, 1977.

Rapp, R., Degree variances of the Earth's gravity, topography and its isostatic compensation, Bull. Geod., 56, 84-94, 1982.

Tapley, B.D., G.H. Born, and M.E. Parke, The SEASAT altimeter data and its accuracy assessment, J. Geophys. Res., 87, 3179-3188, 1982.

Turcotte, D.L., Flexure, Advances in Geophysics, Academic Press, New York, vol. 21, 51-86, 1979.

Walcott, R.I., Flexural rigidity, thickness and viscosity of the lithosphere, J. Geophys. Res., 75, 3941, 3954, 1970.

Watts, A.B., On geoid heights derived from Geos-3 altimeter data along the Hawaiian-Emperor Seamount Chain, J. Geophys. Res., 84, 3817-3826, 1979.

Watts, A.B., and M. Talwani, Gravity anomalies seaward of deep-sea trenches and their tectonic implications, Geophys. J. R. Astron. Soc., 36, 57-90, 1974.

APPENDIX

1. A TEST OF THE MODEL OF UNCOMPENSATED TOPOGRAPHY

Watts and Talwani (1974) proposed a model to explain the relationship between gravity anomalies and topography seaward of deep-ocean trenches. This model which they referred to as the crustal upwarping model (their #3) is essentially the same model as that which we are using in this study (see Figure 1); i.e., the crust and the lithosphere flex as a unit. We wish to test whether this model also can describe the observed relationship between geoid undulations observed from SEASAT and topography. We will represent this relationship in wave number (k) domain by using the admittance function, Z(k); this representation has been popularized for studies of gravity by McKenzie and Bowin (1976) and others. Geoid undulations and bathymetry are characterized, respectively, as output and input signals in a linear system. The spatial Fourier transform of geoid, $\Delta(N)$, is given by

$$F(\Delta N(x)) = Z(k) \cdot F(B(x)) \qquad (A\text{-}1)$$

where F(B(x)) is the Fourier transform of bathymetry. The theoretical admittance function for our crustal upwarping model (Figure 1) is

$$Z(k) = \frac{2\pi G}{g\ k}\ e^{-kd}\ [(\rho_c-\rho_w) + (\rho_m-\rho_w)\ e^{-kt}] \qquad (A\text{-}2)$$

which can be obtained by dividing McKenzie and Bowin's (1976) expression (number 14 for admittance between gravity anomalies and bathymetry) by g k . The theoretical admittance is plotted as a continuous curve in Figure 6. A crustal thickness, t, of 10 km is assumed; all other parameters have the values identical to those which were used in the Model section above.

Figure 6 also shows amplitude estimates of admittance between SEASAT observations of sea surface height and ocean depths interpolated from NORDA digitized bathymetry. These estimated admittances are obtained from 23 SEASAT passes over the Aleutian trench (see Figure 2a). For each pass a sequence of the 128 (2^7) data points just seaward of the trench axis is formed. A mean was removed from each sequence and a degree-and-order 12 background geoid was subtracted from each height profile. The 23 sequences were then combined into a single sequence of SEASAT data; a corresponding bathymetric sequence was also formed. After the fashion of McKenzie and Bowin (1976) admittance estimates were obtained from the ratio of cross-spectral estimates to the bathymetric power spectral estimates. To obtain estimates of the cross spectrum, Welch's method of averaged modified periodogram was used in conjunction with fast Fourier transform algorithms.

The estimated admittances in Figure 6 agree reasonably well with theoretical admittances thereby supporting the popular assumption that topography of the Outer Rise is uncompensated. The crustal upwarping model is consistent with the admittances estimated from SEASAT data. Admittances estimated from altimeter data over mid-plate (compensated) topography (Watts, 1979) are much less at wavelengths in the range 300 to 1000 km.

Acknowledgements

We are grateful to R. Kolenkiewicz for valuable discussions and for bathymetry data which he kindly provided. We also thank S. Poulose for all the help she gave us with the computer. S. Klosko helped with the background gravity model. Fruitful discussions with G. Sharman and R. Williamson are also gratefully acknowledged.

TABLE I

Trench	Flexural Wavelength α(km)	Amplitude w_b(m)	Elastic Thickness T_e(km)	Age (10^6 Yr)
Mariana (9)	107.9	465.± 75.	51.3±0.3	140-160
Kuril (22)	92.7	513.±139.	41.9± 5.1	100-110
Aleutian (20)	90.8	461.±61.	35.4± 1.4	52- 65
Philippines (8)	66.3	307.±74.	26.8± 4.3	50- 55
Middle Amer (14)	71.7	322.±46.	29.7± 2.4	22- 30
Bonin (4)	126.0	354.±20.	63.0± 8.6	135-160

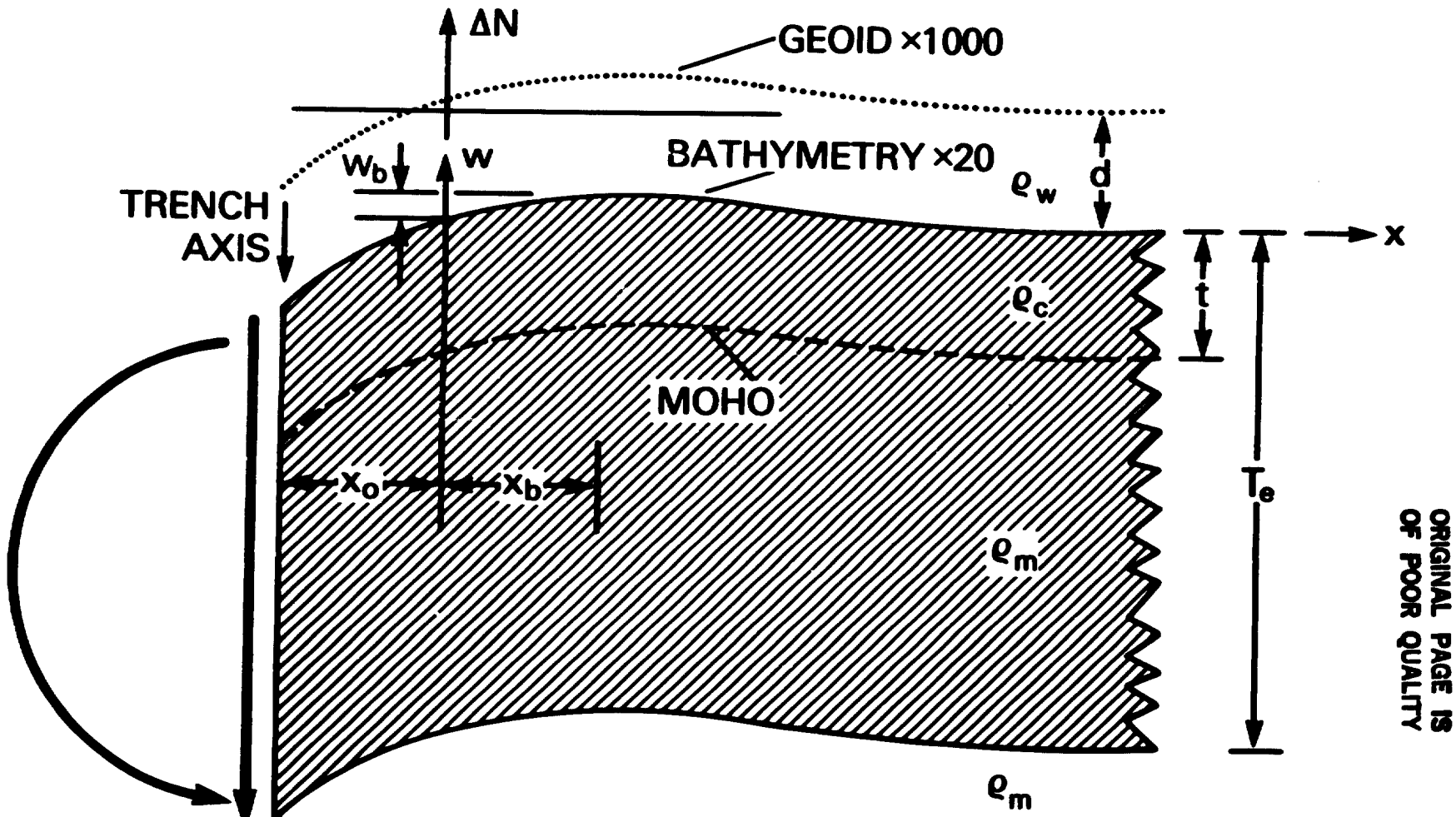

Figure 1. Model of end-loaded elastic lithospheric plate overlying a fluid-like asthenospheric substrate. Crust and lithosphere deflect as a unit. Modal outputs include seafloor deflection profile, w(x), and concommitant profile of geoid heights, ΔN(x).

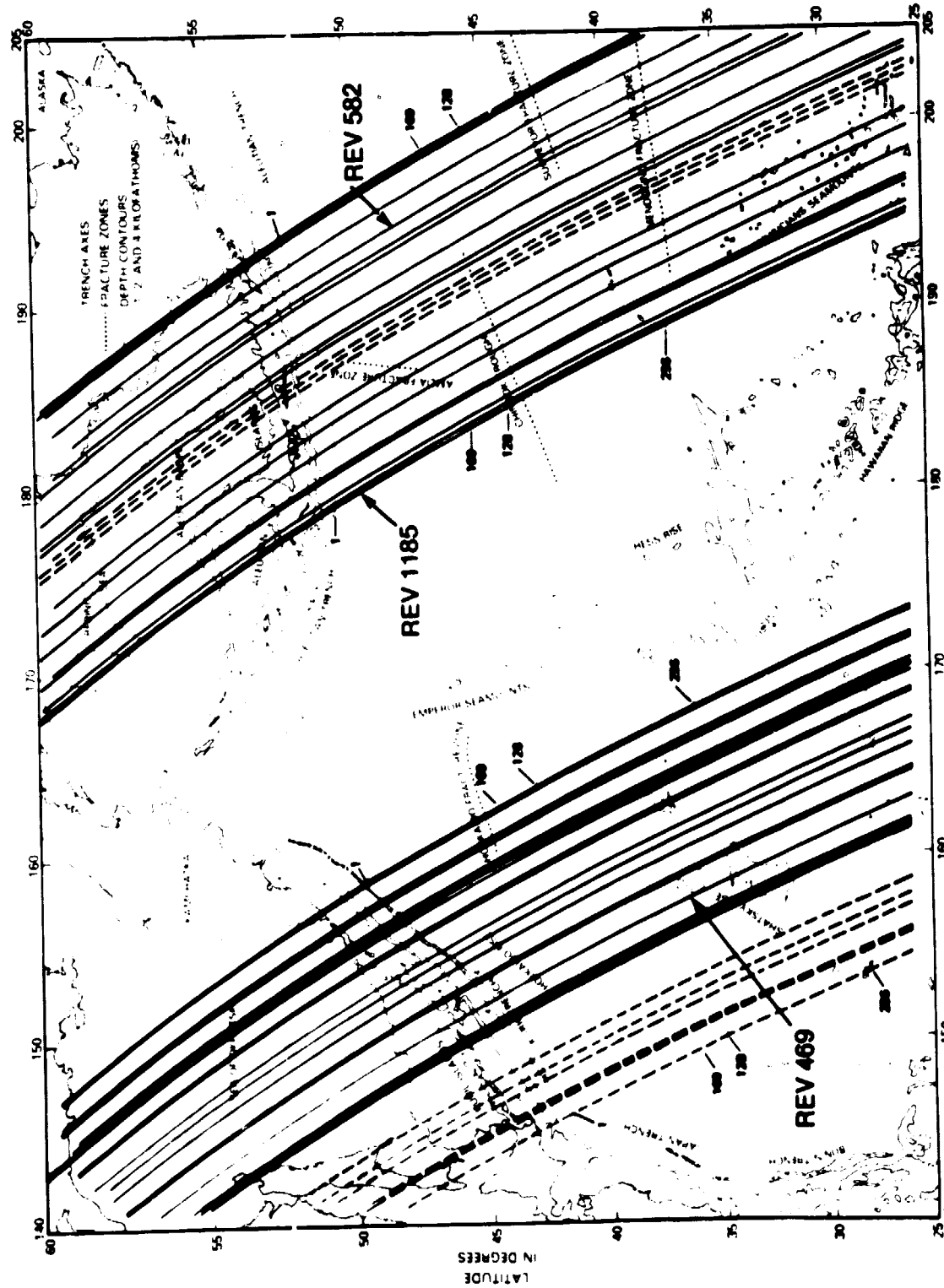

Figure 2a. Groundtracks of SEASAT passes analyzed over the Kuril and Aleutian trenches. Dashed lines represent groundtracks of passes which were analyzed but culled (see text). Solid lines are groundtracks of retained passes. Altimeter data analyzed lies between trench axis (1) and 100 sec (100) prior to axis.

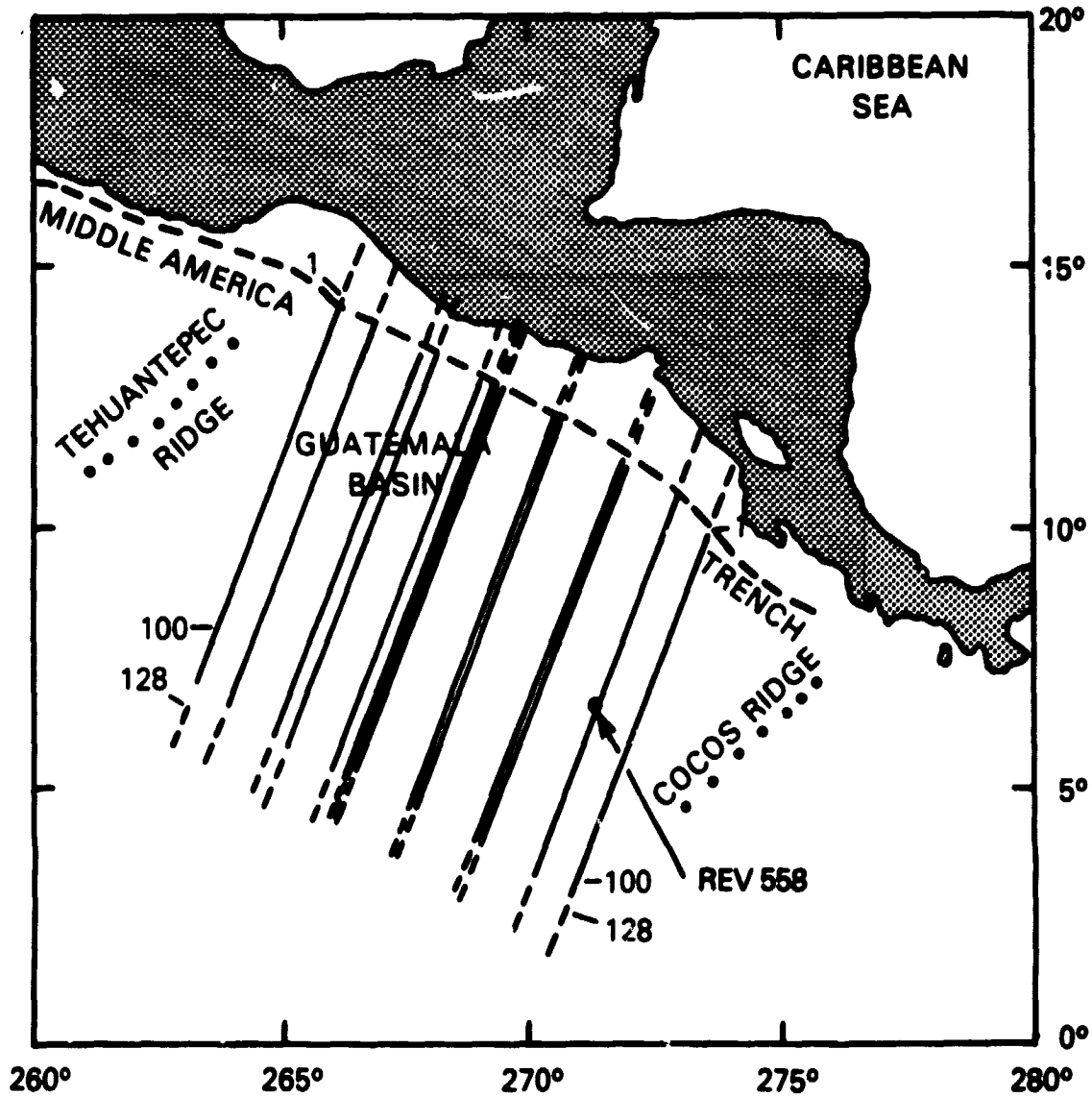

Figure 2b. Groundtracks of SEASAT passes analyzed over the Middle America trench. See text.

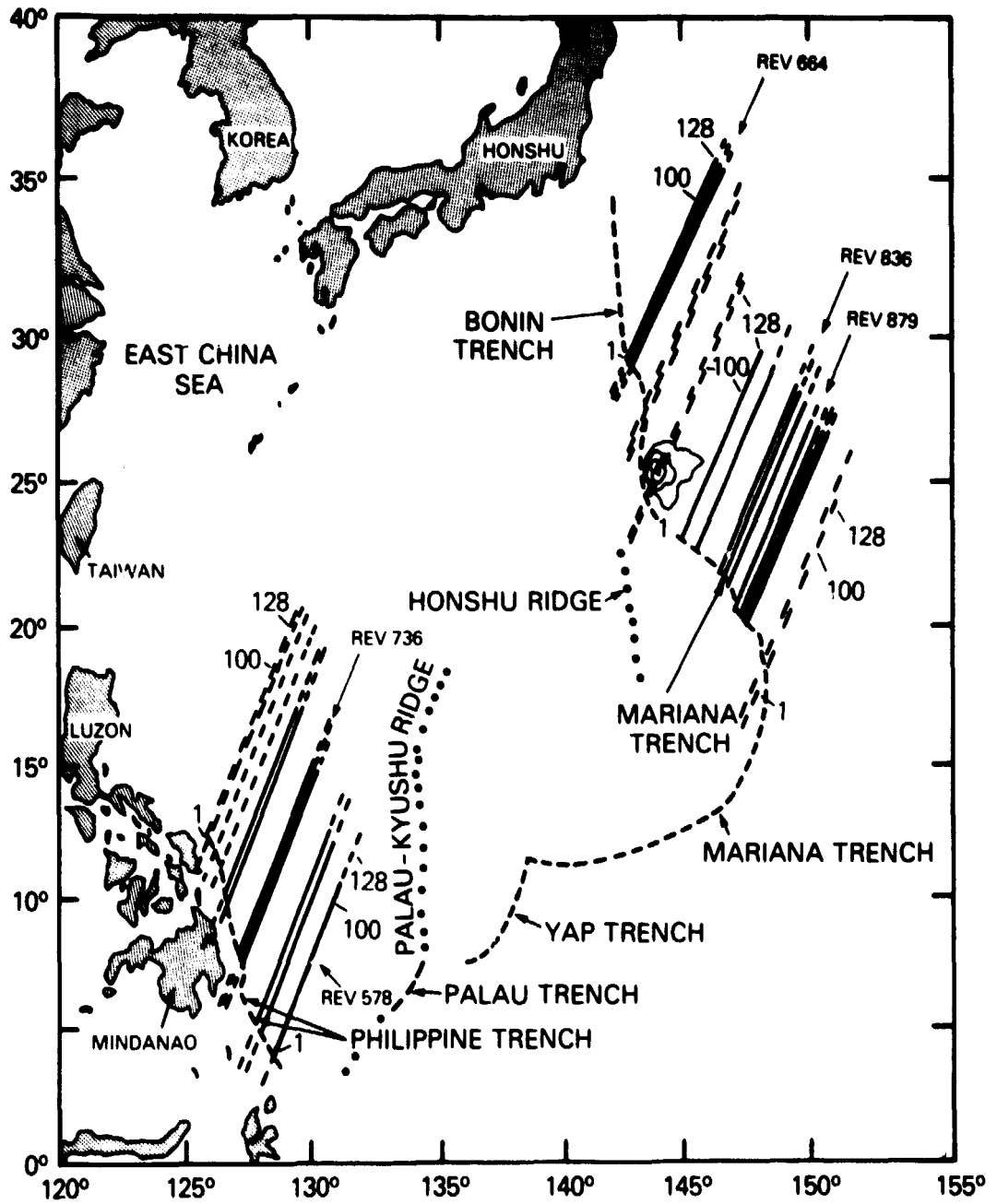

Figure 2c. Groundtracks of SEASAT passes analyzed over the Philippine, Izu-Bonin and Mariana trenches. See caption for Figure 2a.

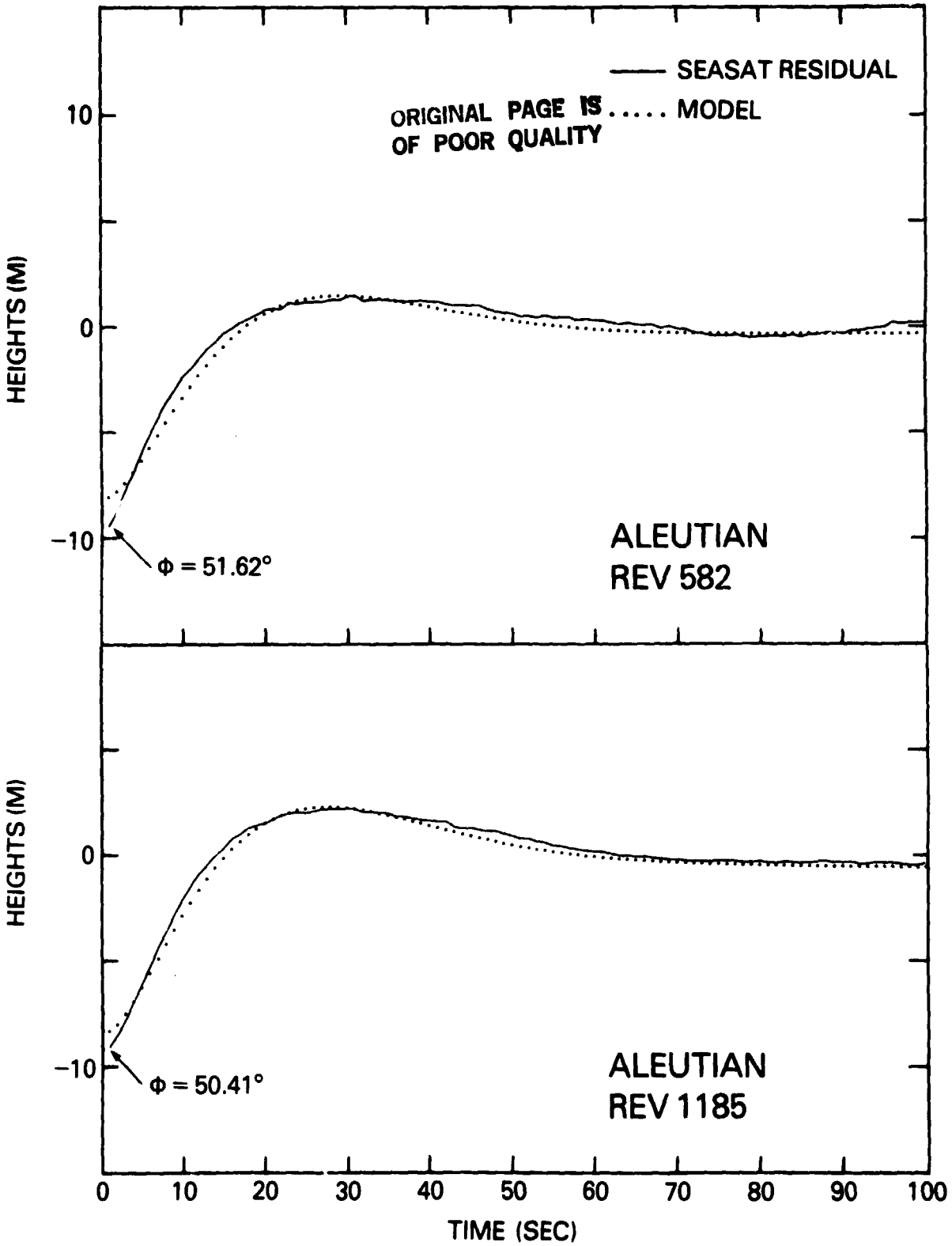

Figure 3a-3b. Selected SEASAT passes over trenches indicated. Residual sea surface heights (with degree-and-order 48 background geoid removed) shown as solid curves. Best-fitting theoretical geoid profiles from elastic plate model are shown as dotted curves.

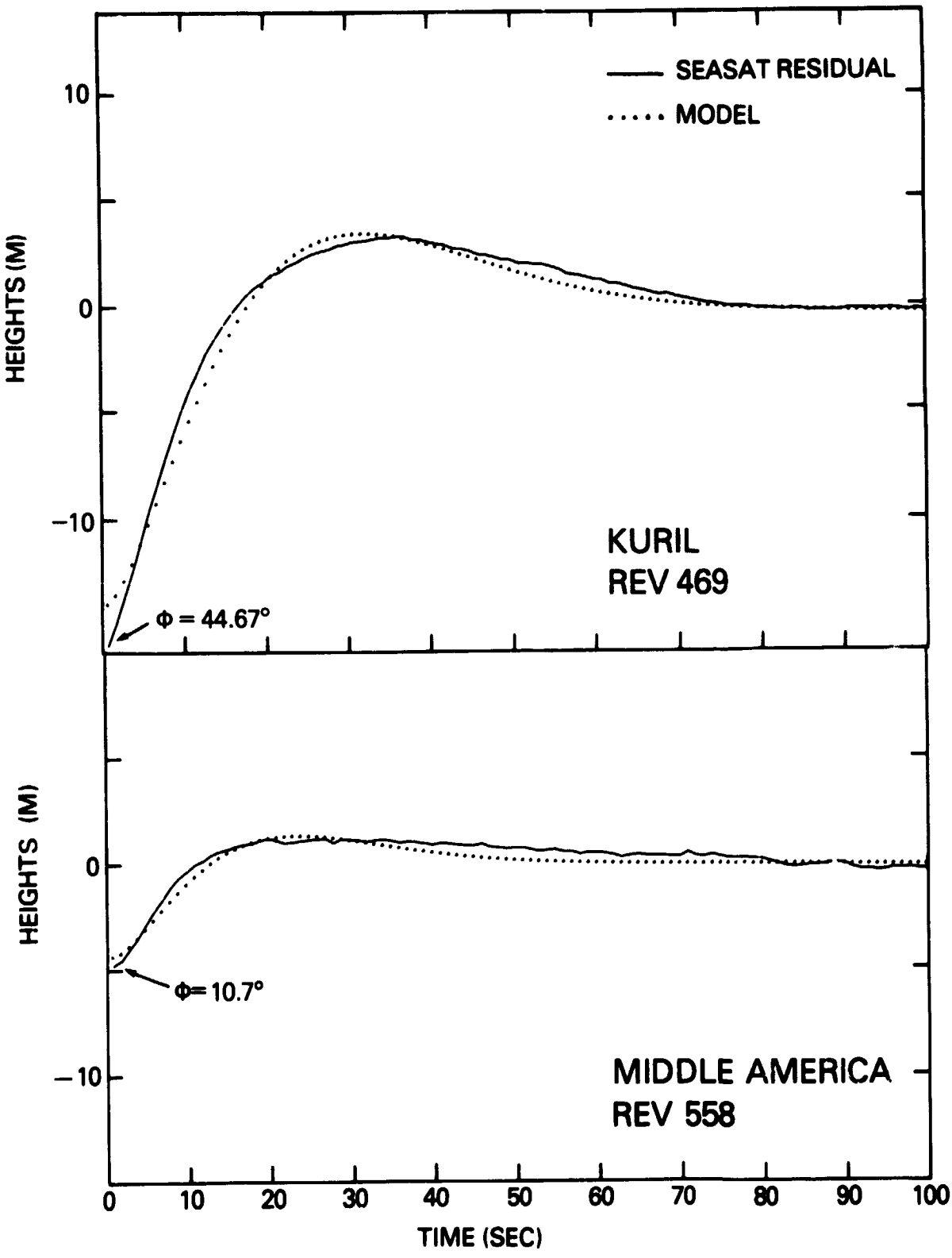

Figure 3c-3d. Selected SEASAT passes over trenches indicated. Residual sea surface heights (with degree-and-order 48 background geoid removed) shown as solid curves. Best-fitting theoretical geoid profiles from elastic plate model are shown as dotted curves.

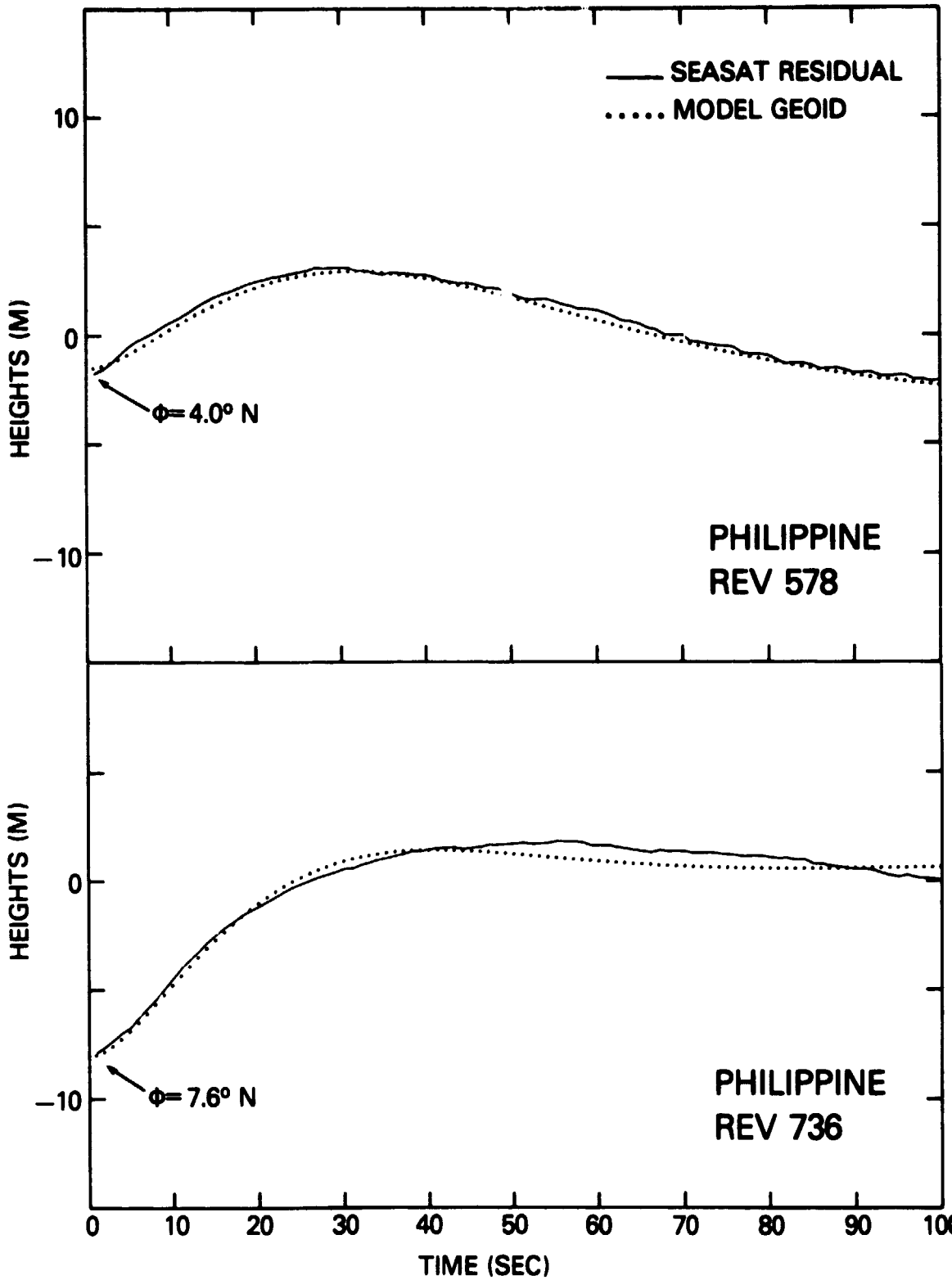

Figure 3e-3f. Selected SEASAT passes over trenches indicated. Residual sea surface heights (with degree-and-order 48 background geoid removed) shown as solid curves. Best-fitting theoretical geoid profiles from elastic plate model are shown as dotted curves.

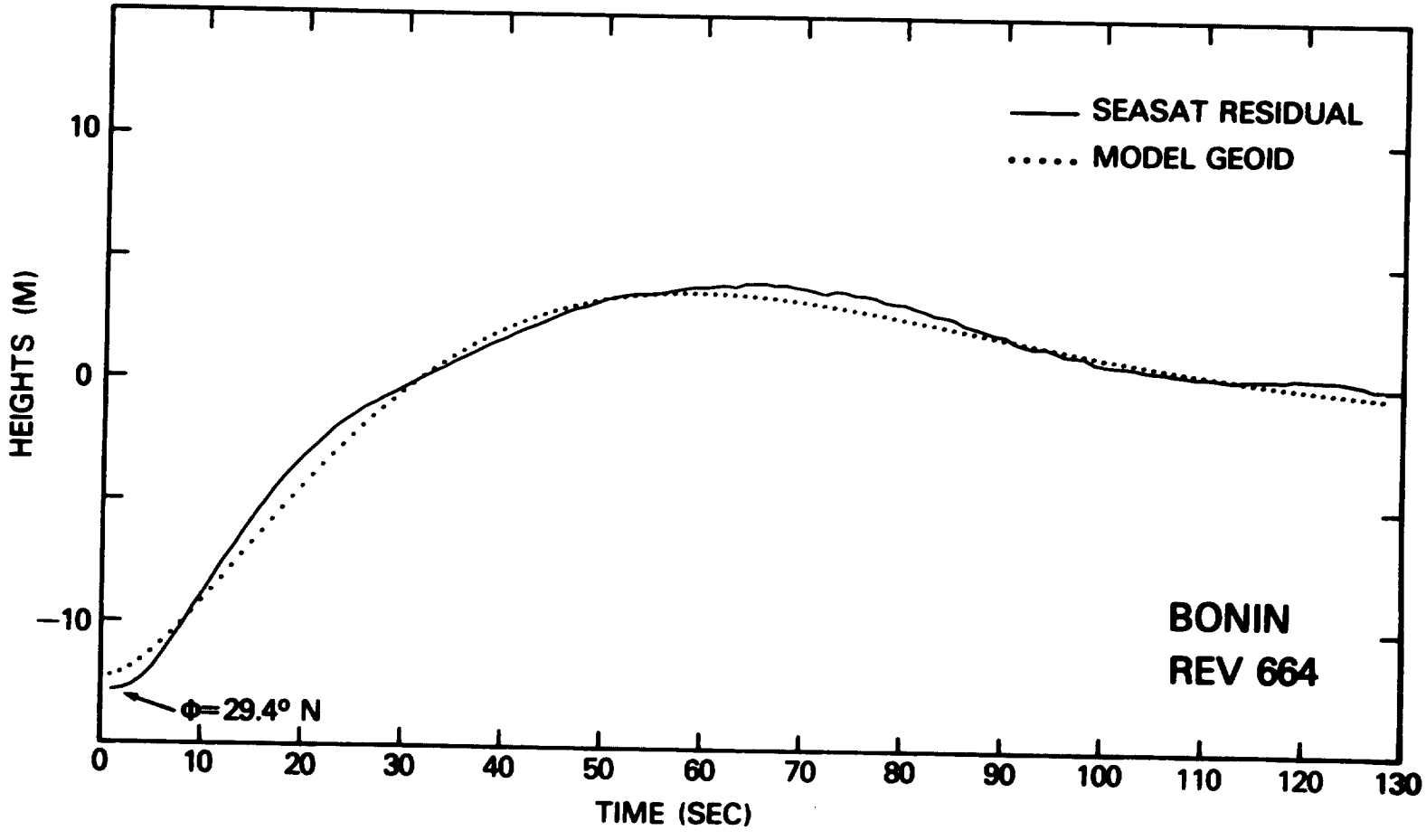

Figure 3g. Selected SEASAT passes over trenches indicated. Residual sea surface heights (with degree-and-order 48 background geoid removed) shown as solid curves. Best-fitting theoretical geoid profiles from elastic plate model are shown as dotted curves.

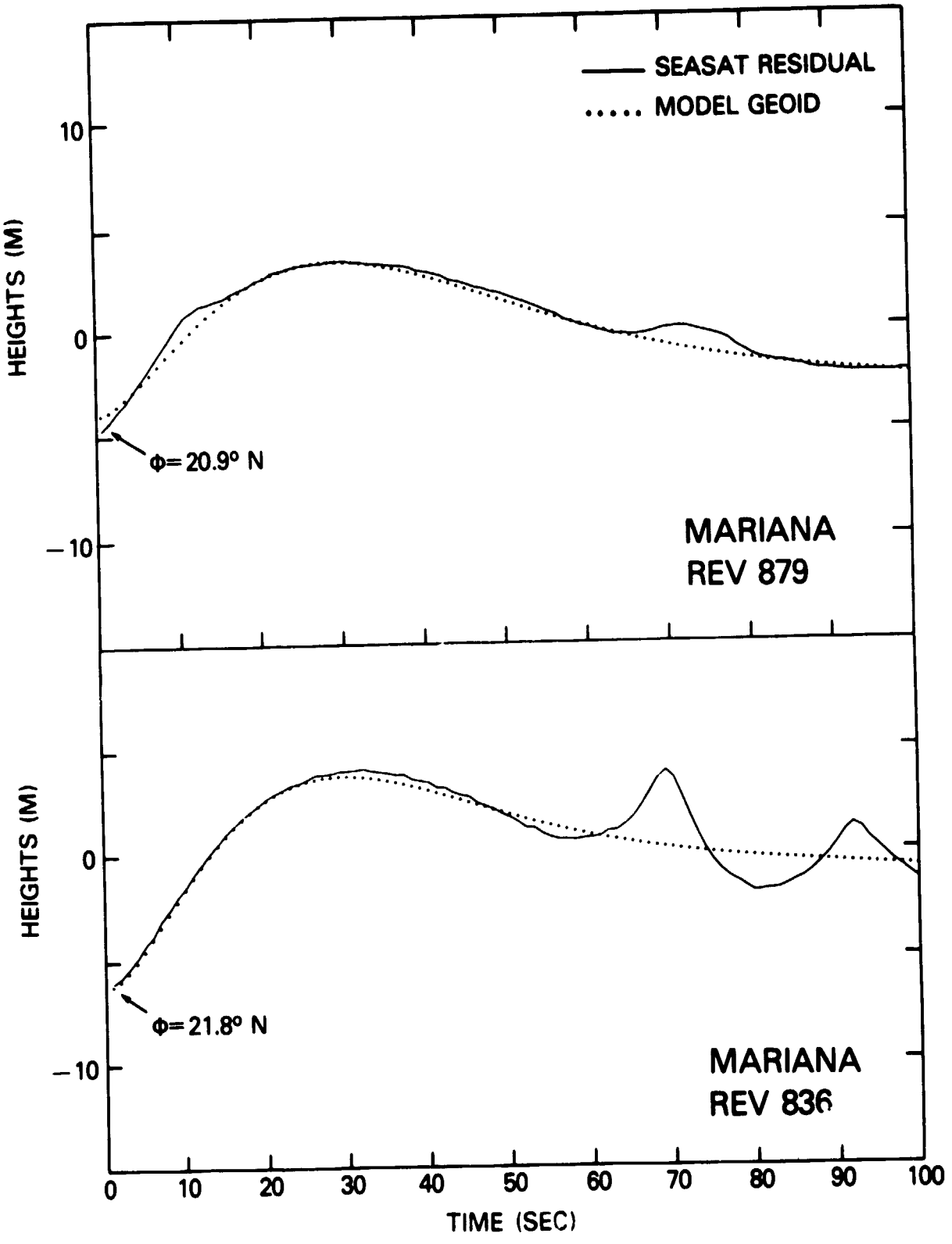

Figure 3h-3i. Selected SEASAT passes over trenches indicated. Residual sea surface heights (with degree-and-order 48 background geoid removed) shown as solid curves. Best-fitting theoretical geoid profiles from elastic plate model are shown as dotted curves.

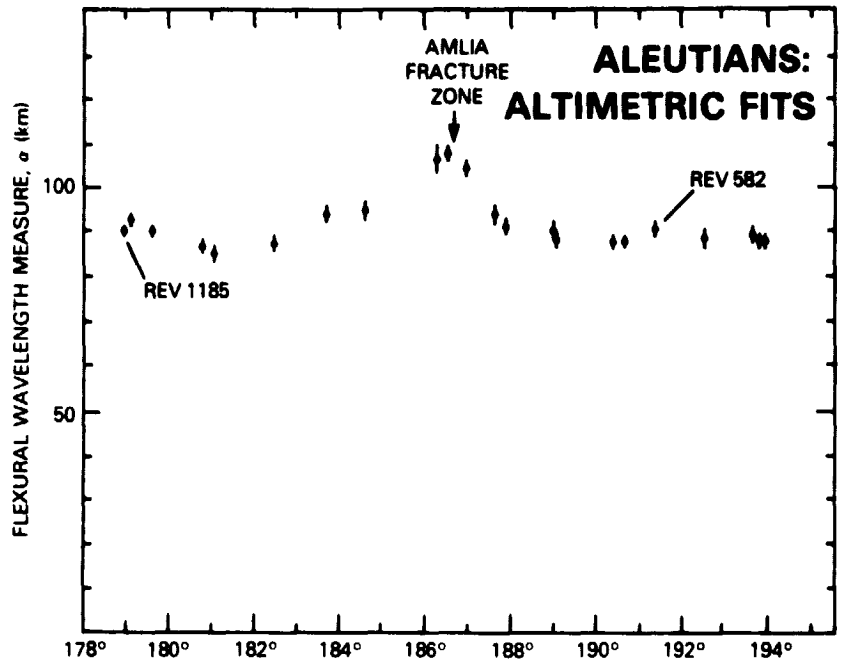

Figure 4a. Values of flexural wavelength, α_u, estimated for each of 23 SEASAT passes over the Aleutian trench plotted vs longitude of intersection between trench axis and groundtrack.

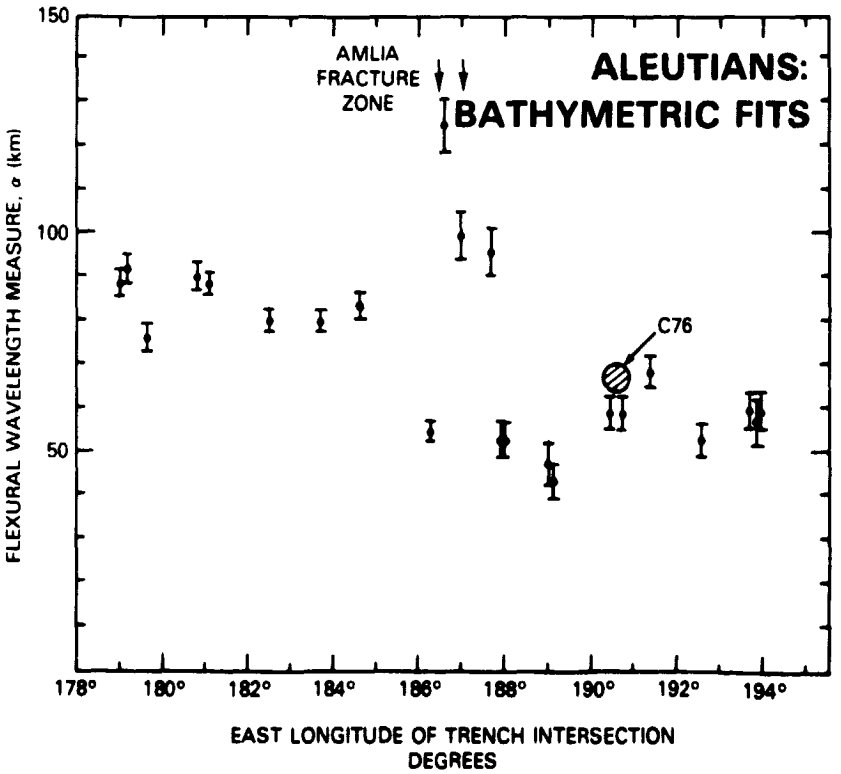

Figure 4b. Values of flexural wavelength, α_u, estimated for 23 interpolated bathymetric profiles coinciding with 23 SEASAT passes used in Figure 4a.

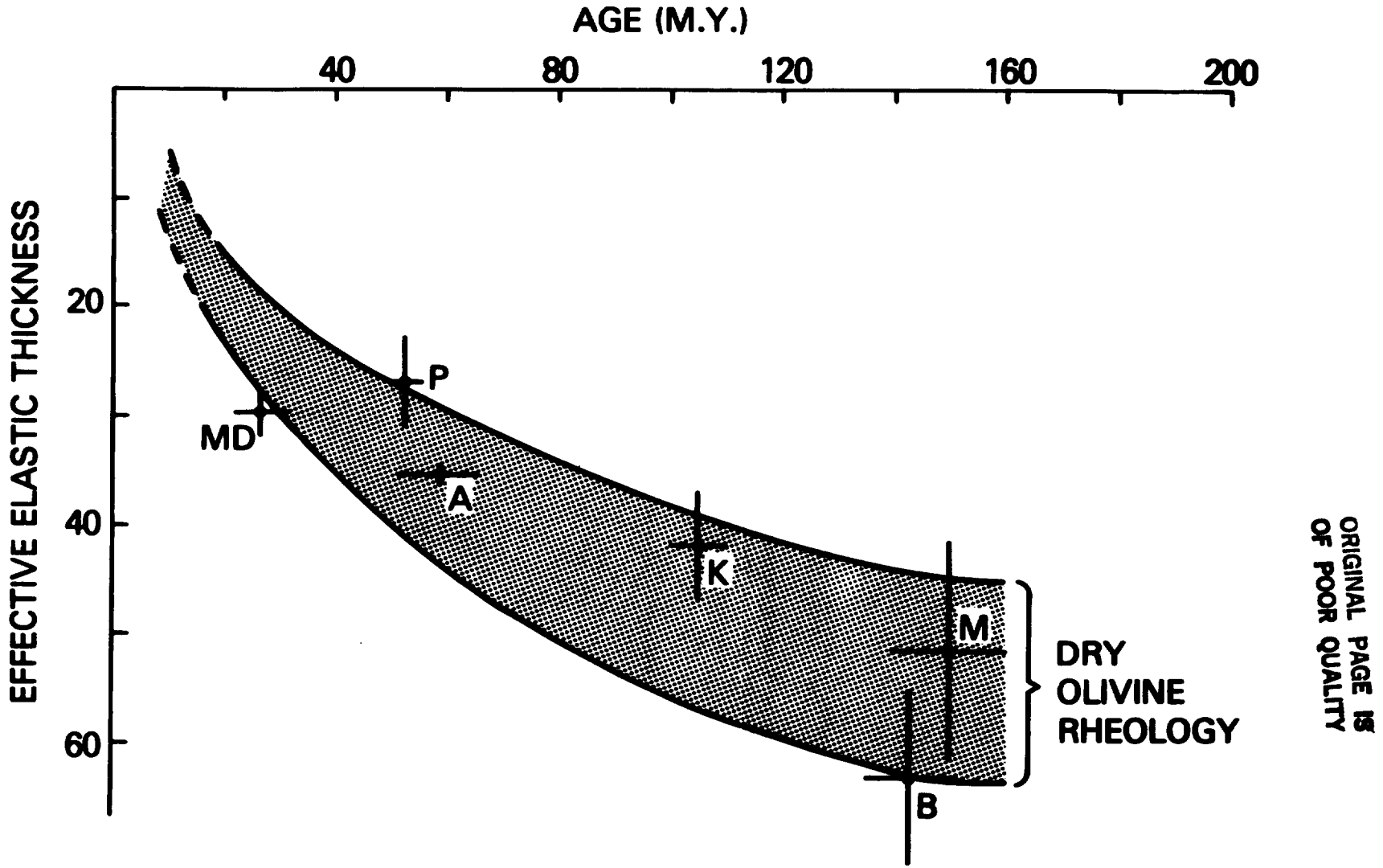

Figure 5. Effective elastic thickness (EET) derived from SEASAT data (crosses) over six trenches. Middle American (MD), Aleutian (A), Philippine (P), Kuril (K), Mariana (M) and Bonin (B). EET's are plotted versus age. Bodine et al. (1981) age-thickness relation (9) is shown as curves; see text.

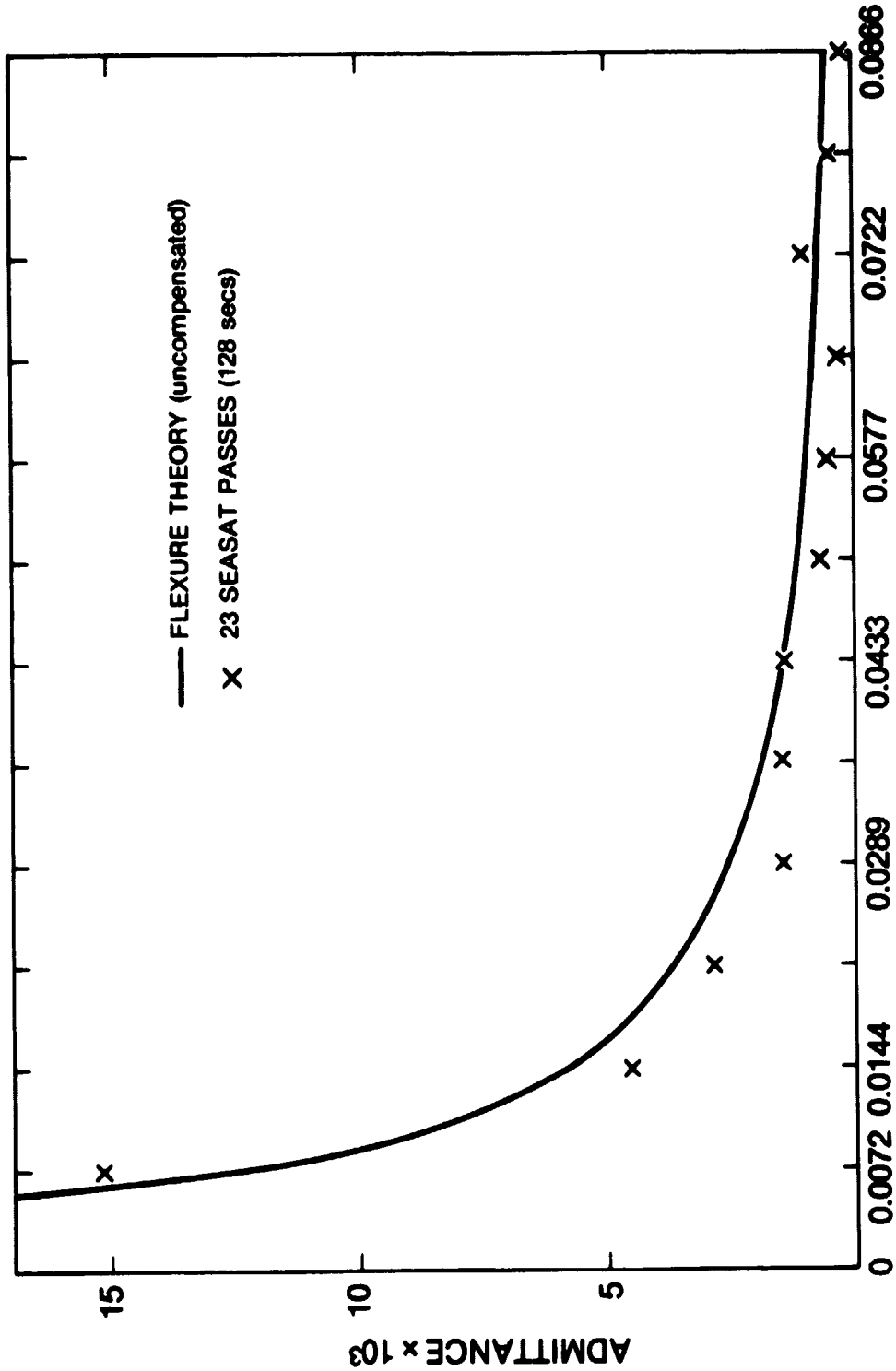

Figure 6. Estimates of admittance Z(k), in meters per meter, between geoid heights and bathymetry for ensemble of 23 SEASAT passes across the Aleutian trench. Theoretical admittance from flexure model (equation A-2) is shown as a solid curve. See text.